Test of classical nucleation theory on deeply supercooled high-pressure simulated silica

Ivan Saika-Voivod
Department of Chemistry, University of Saskatchewan, Saskatoon, Saskatchewan S7N 5C9, Canada

Peter H. Poole
Department of Physics, St. Francis Xavier University, Antigonish, Nova Scotia B2G 2W5, Canada

Richard K. Bowles[a)]
Department of Chemistry, University of Saskatchewan, Saskatoon, Saskatchewan S7N 5C9, Canada

(Received 24 January 2006; accepted 18 April 2006; published online 13 June 2006)

We test classical nucleation theory (CNT) in the case of simulations of deeply supercooled, high density liquid silica, as modeled by the van Beest–Kramer–van Santen potential [Phys. Rev. Lett. **64**, 1995 (1990)]. We find that at density $\rho=4.38$ g/cm^3, spontaneous nucleation of crystalline stishovite occurs in conventional molecular dynamics simulations at temperature $T=3000$ K, and we evaluate the nucleation rate J directly at this T via "brute force" sampling of nucleation events in numerous independent runs. We then use parallel, constrained Monte Carlo simulations to evaluate $\Delta G(n)$, the free energy to form a crystalline embryo containing n silicon atoms, at $T=3000$, 3100, 3200, and 3300 K. By comparing the form of $\Delta G(n)$ to CNT, we test the ability of CNT to reproduce the observed behavior as we approach the regime where spontaneous nucleation occurs on simulation time scales. We find that the prediction of CNT for the n dependence of $\Delta G(n)$ fits reasonably well to the data at all T studied. $\Delta\mu$, the chemical potential difference between bulk liquid and stishovite, is evaluated as a fit parameter in our analysis of the form of $\Delta G(n)$. Compared to directly determined values of $\Delta\mu$ extracted from previous work, the fitted values agree only at $T=3300$ K; at lower T the fitted values increasingly overestimate $\Delta\mu$ as T decreases. We find that n^*, the size of the critical nucleus, is approximately ten silicon atoms at $T=3300$ K. At 3000 K, n^* decreases to approximately 3, and at such small sizes methodological challenges arise in the evaluation of $\Delta G(n)$ when using standard techniques; indeed even the thermodynamic stability of the supercooled liquid comes into question under these conditions. We therefore present a modified approach that permits an estimation of $\Delta G(n)$ at 3000 K. Finally, we directly evaluate at $T=3000$ K the kinetic prefactors in the CNT expression for J, and find physically reasonable values; e.g., the diffusion length that Si atoms must travel in order to move from the liquid to the crystal embryo is approximately 0.2 nm. We are thereby able to compare the results for J at 3000 K obtained both directly and based on CNT, and find that they agree within an order of magnitude. In sum, our work quantifies how certain predictions of CNT (e.g., for $\Delta\mu$) break down in this deeply supercooled limit, while others [the n dependence of $\Delta G(n)$] are not as adversely affected. © *2006 American Institute of Physics*. [DOI: 10.1063/1.2203631]

I. INTRODUCTION

In recent years, computer simulations have increasingly been used to study the nucleation and growth of crystals from the supercooled liquid state. Molecular dynamics (MD) simulations have been particularly useful in testing, on a molecular level, the predictions of classical nucleation theory (CNT).[1–6] In large measure, this has been made possible by the development of novel computational techniques that permit the determination, from simulations, of free energy barriers, kinetic prefactors, and the order parameters required to quantitatively test the predictions of CNT.[7–11] A key feature of these techniques is that they allow the study of nucleation under thermodynamic conditions at which spontaneous crystal nucleation does not occur on the short physical time scales accessible to conventional MD simulations. As a consequence, much previous work has focused on testing CNT, and calculating the nulcleation rate, at low to intermediate degrees of supercooling, where CNT is expected to best apply.

At the same time, spontaneous crystal nucleation is observed in a number of simulated liquid systems under very highly supercooled conditions where the nucleation time is comparable to or less than the simulation time scale (e.g., Refs. 12–16). Current conventional MD simulations typically are able to study systems of a few thousand molecules over a time scale of tens of nanoseconds. Within these restrictions, a spontaneously crystallizing system will exhibit quite small crystal nuclei compared to those found at higher temperature T, and it is generally expected that CNT will not predict well the behavior of the system in this regime. Con-

a)Electronic mail: richard.bowles@usask.ca

sequently, relatively few studies examine this deeply supercooled limit of nucleation behavior in the context of CNT.

The purpose of the present work is to explore this deeply supercooled limit of nucleation behavior, with the goal of testing the limits of CNT and quantifying how the theory begins to fail in this regime; and also to determine the technical limits of applicability of the simulation methods usually employed at higher T. We are interested in determining if it is possible to compare a nucleation rate calculated using CNT, and a rate found directly from a spontaneously crystallizing MD simulation. The latter question is particularly interesting, since only a few simulation studies compare nucleation rates found from CNT to a rate calculated independently,[8,11,17] yet such comparisons are a key tool for developing and testing improved theoretical descriptions of nucleation.

To achieve these goals, we study liquid silica as modeled by the van Beest–Kramer–van Santen (BKS) potential.[18] The thermodynamic and transport properties of the supercooled liquid state of this model have been characterized in detail.[19,20] Previous work has also evaluated the phase diagram of the system, providing the coexistence conditions demarcating the liquid, and several crystalline phases.[21] Most significant for the current purpose, we find that the liquid spontaneously crystallizes to stishovite[22] in our simulations when cooled to approximately $T=3000$ K at a density $\rho=4.38$ g/cm^3. The liquid at this T exhibits the two-step relaxation in its dynamical quantities characteristic of a deeply supercooled fluid, but it is still diffusive enough to reach metastable equilibrium on a time scale much shorter than the time scale for crystal nucleation. Consequently, we are able to make a direct calculation of the rate at 3000 K using an ensemble of independent MD simulations, while at the same time, we can determine the properties of the metastable liquid.

We also use constrained Monte Carlo simulations of the liquid to calculate the free energy barrier to nucleation at the same density, over a range of temperatures from 3000 to 3300 K, to test the degree to which the predictions of CNT are satisfied on approaching $T=3000$ K. The key predictions of CNT we wish to test relate to the central quantity of the theory, $N(n)$, the equilibrium cluster size distribution, or the number of clusters containing n particles.[6] In this work, we will track Si atoms only, and assume from stoichiometry that a cluster nominally of size n (n Si atoms) actually contains $3n$ atoms (n Si atoms and $2n$ O atoms). $N(n)$ is interpreted to yield the work $\Delta G(n)$ of forming a cluster of size n from the surrounding metastable liquid via

$$\frac{\Delta G(n)}{k_B T} = -\ln\left[\frac{N(n)}{N(0)}\right], \tag{1}$$

where $N(0)$ is the number of liquidlike Si atoms; so defined $\Delta G(0)=0$. Whether the distribution of cluster sizes is extensive or intensive (i.e., normalized or not), the barrier is system size independent. Within the CNT framework, the phenomenological model for the work is given by

$$\Delta G(n) = -|\Delta\mu| n + a n^{2/3}, \tag{2}$$

where $\Delta\mu=\mu_{\text{stish}}-\mu_{\text{liq}}$ is the difference in chemical potential between the bulk stable and metastable phases, and a is a surface term that is proportional to the surface tension γ and depends on the shape of the nuclei. At a critical cluster size n^*, $\Delta G(n)$ has a maximum and clusters larger than n^* will grow spontaneously, forming the new phase. $\Delta G(n^*)$ then represents the free energy barrier to nucleation. In this study, we use computer simulation techniques that connect $\Delta G(n)$ with the probability of appearance of an n-sized cluster within the simulation, where the cluster is identified by a specific cluster criterion.[7,10,23] We can then compare our barrier calculations with the general form suggested by Eq. (2).

According to CNT, the rate of nucleation, i.e., the rate at which critical nuclei go over the barrier, is

$$J^{\text{CNT}} = K \exp\left(-\frac{\Delta G(n^*)}{k_B T}\right), \tag{3}$$

where the kinetic prefactor is given by

$$K = 24\rho_n Z D n^{*2/3}/\lambda^2 \tag{4}$$

$$= \rho_n Z f^+_{\text{crit}}, \tag{5}$$

where $Z=\sqrt{|\Delta\mu|/6\pi k_B T n^*}$ is the Zeldovich factor, D is the diffusion constant, k_B is the Boltzmann constant, ρ_n is the number density of particles, λ is a typical distance particles must diffuse in order to go from the metastable liquid to the embryonic cluster, and f^+_{crit} is the rate at which particles are added to the critical nucleus. We note that the use of f^+_{crit} is an innovation introduced in Ref. 10. In the case of diffusive barrier crossing f^+_{crit} can be calculated from simulation via

$$f^+_{\text{crit}} = \frac{1}{2}\frac{\langle[n^*(t)-n^*(0)]^2\rangle}{t}, \tag{6}$$

where $\langle\cdot\rangle$ denotes an ensemble average.

Our Monte Carlo simulations of liquid silica between 3300 and 3000 K show that CNT describes the liquid well at the highest T, but that deviations in the observed and predicted behaviors emerge at lower T. At the lowest T, we also identify technical difficulties associated with obtaining $N(n)$ and we describe an alternative strategy that at least partially addresses them. Notwithstanding these challenges, at the lowest $T=3000$ K, we are still able to calculate the kinetic prefactors for the nucleation rate as described in CNT, so that we can compare the predicted rate to that calculated from direct MD simulations. Despite the worsening correspondence between our results and the thermodynamic aspects of CNT at low T, the rates compare reasonably well. Whether the correspondence of the rates at this large degree of supercooling is peculiar to our system or whether this is a general result is an open question. We also find that $N(n)$, as obtained for the equilibrium system (i.e., the system that samples the equilibrium distribution of embryos, including those embryos near to, at, and beyond the nucleation barrier), is different from the analogous quantity for the metastable liquid state (i.e., the metastable equilibrium sampled in a conven-

tional MD simulation prior to the onset of nucleation), raising the question of which distribution is more significant in determining the rate.

In Sec. II, we describe the model system. Section III describes the direct MD nucleation rate calculation, while Sec. IV describes the CNT calculations and explores the use of the metastable liquid in determining the free energy barrier. We subsequently present our discussion and conclusions in Secs. V and VI, respectively. The Appendix describes our methods and criteria for defining a crystalline cluster.

II. SYSTEM OF STUDY

We study a system of 444 Si and 888 O ions governed by a modified BKS potential and in a cubic simulation cell with periodic boundaries. The modification includes a short range additive patch to prevent "fusion" events, and a tapering of the real space part of the potential with a polynomial tail so that it smoothly reaches zero at 1 nm. Long range forces are handled via the Ewald summation. The details of the potential are given in Ref. 20.

The phase diagram of BKS silica has been recently evaluated in Ref. 21 (Fig. 1). In that work, the stability fields of the liquid, stishovite, β-quartz, and coesite have been determined. In this study we focus on the molar volume $V=V_0=4.5733$ cm^3/mol ($\rho=4.3793$ g cm^{-3}) liquid isochore, which, as shown in Fig. 1(b), falls in the one-phase stability field of stishovite. A view of stishovite along the c axis showing Si atoms only is provided in Fig. 2. In stishovite, there are six O atoms surrounding each Si atom in an octahedral arrangement. These octahedra, connected along edges and at corners, arrange themselves in a compact manner.

We perform our simulations in the NVT ensemble, where N is the number of molecules. Usually, nucleation experiments and simulations are done at constant pressure P. However, we find that for the state points of interest, the critical nuclei we observe are small and do not noticeably change the P of the system. Only once the crystallization process advances well into the growth stage does P or the potential energy U of the system change significantly. Therefore, the critical nucleus forms within a liquid that is characterized to a good approximation either by the system's P or V. However, the density of the nucleus itself is not known. Hence, we also show in Fig. 1(b) the V of bulk stishovite at the pressure at which the liquid is studied.

P and U are needed along the V_0 isochore to determine $\Delta\mu$, which we obtain by extending the calculations described in Ref. 21. The diffusion coefficient is also needed in order to calculate the kinetic prefactor. To obtain these quantities, we perform MD simulations at constant V in both the liquid and stishovite, near and along V_0. First we equilibrate the system near the desired T with simple velocity scaling every 100 time steps, and then we allow the system to continue in the NVE ensemble for about 1 ns (E is the total energy). For the $T=3000$ K and $T=3100$ K cases, numerous independent runs are performed, and only those that do not show any signs of crystallizing are used to determine the desired quantities.

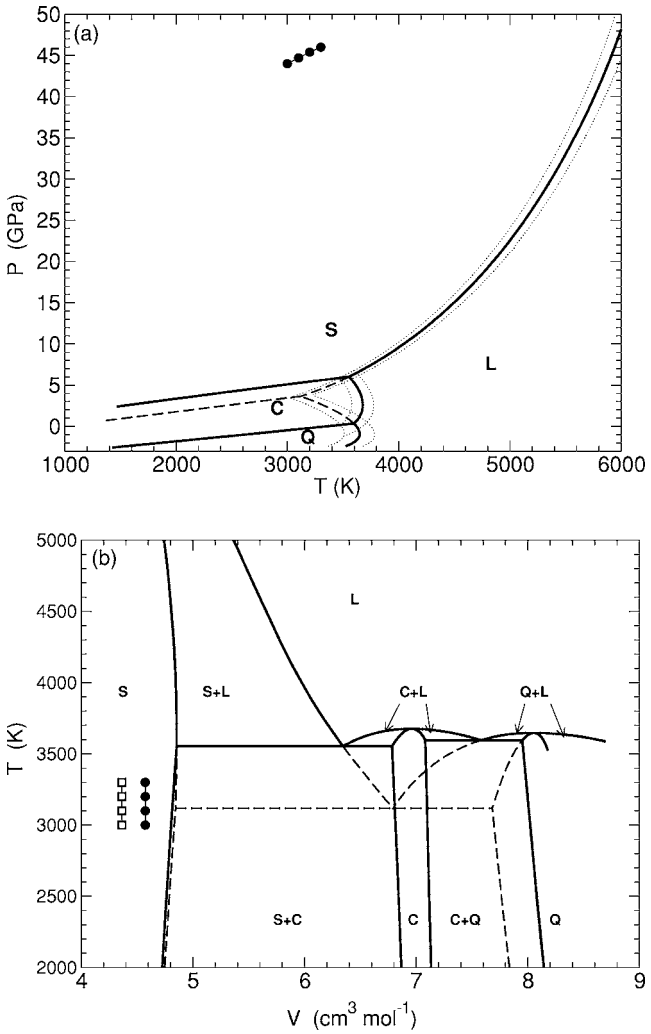

FIG. 1. Location of studied liquid state points (filled circles) in the (a) PT and (b) VT phase diagrams of BKS silica. At a given P and T, stishovite has a higher density than that of the liquid. Therefore, we also plot the stishovite state points corresponding to the liquid P (open squares) in (b). The phases shown in the diagrams are the liquid (L), β-quartz (Q), coesite (C), and stishovite (S). (b) At fixed V, thermodynamic ground states are often mixtures of two coexisting phases. The liquid state points studied fall within the one-phase stability field of stishovite. Despite the proximity of our chosen state points to the stishovite to stishovite-plus-coesite boundary in the VT plane, the location in the PT plane is deep within the stishovite region. The dashed lines are metastable extensions of stishovite and β-quartz transitions, and the dotted lines represent the uncertainty in the location of the melting lines. V is given per mol ion.

For the liquid at $T=T_0=3000$ K and V_0, the Si diffusion coefficient is $D=8.04\pm0.2\times10^{-7}$cm^2 s^{-1} as determined from the slope of the mean squared displacement of Si atoms as a function of time t, and the pressure is found to be $P_0=44.0$ GPa. This and higher T state points are shown to be in the stishovite stability field in the PT phase diagram [Fig. 1(a)].

At P_0, stishovite has a lower molar volume ($V=4.364$ cm^3 mol^{-1}) than the melt. The stishovite state points corresponding to the pressure of the liquid [shown in Fig. 1(b)] are the state points used to calculate $\Delta\mu$: $\Delta\mu$ is calculated between the two phases at the same P, for which (in general) the volumes are different.

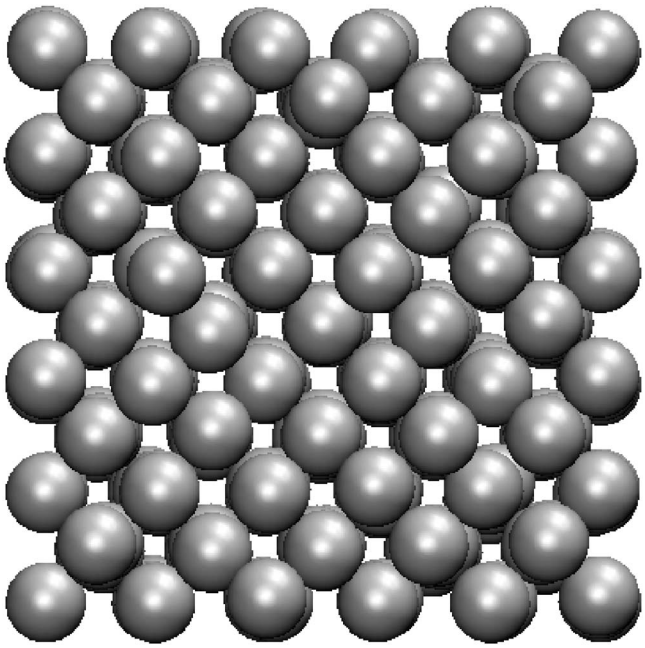

FIG. 2. Stishovite at 3000 K, as viewed down the crystallographic c axis. Only Si atoms are shown.

III. NUCLEATION RATE FROM MD SIMULATIONS

We use MD simulations in the *NVT* ensemble to calculate the nucleation rate at T_0 and V_0 in a "brute force" way. We first equilibrate the liquid at 5000 K, and then quench 198 independent configurations to 3000 K, employing the Berendsen thermostat[24] with a time constant of 1 ps. Other simulation details are the same as given in the previous section. The simulation continues at 3000 K until the system crystallizes.

Figure 3(a) shows two sample time series, illustrating a large drop in potential energy associated with the phase change. Figure 3(b) shows the components of the radial distibution function $g(r)=g_{\mathrm{SiSi}}(r)+2g_{\mathrm{SiO}}(r)+g_{\mathrm{OO}}(r)$ for the metastable liquid (i.e., when the time series is stable), the crystallized system, and pure stishovite at T_0. The comparison of each $g(r)$ shows that we indeed crystallize to stishovite.

Figure 3(c) shows $F_{\mathrm{SiSi}}(q,t)$, the dynamic structure factor at fixed wave number q obtained by considering only Si atoms (which diffuse more slowly than O), obtained from the metastable liquid portion of a simulation before the onset of crystallization. As a reference for the three wave numbers chosen, we plot the static structure factor $S(q)$ in the inset. We do not observe any time evolution of $S(q)$ during the

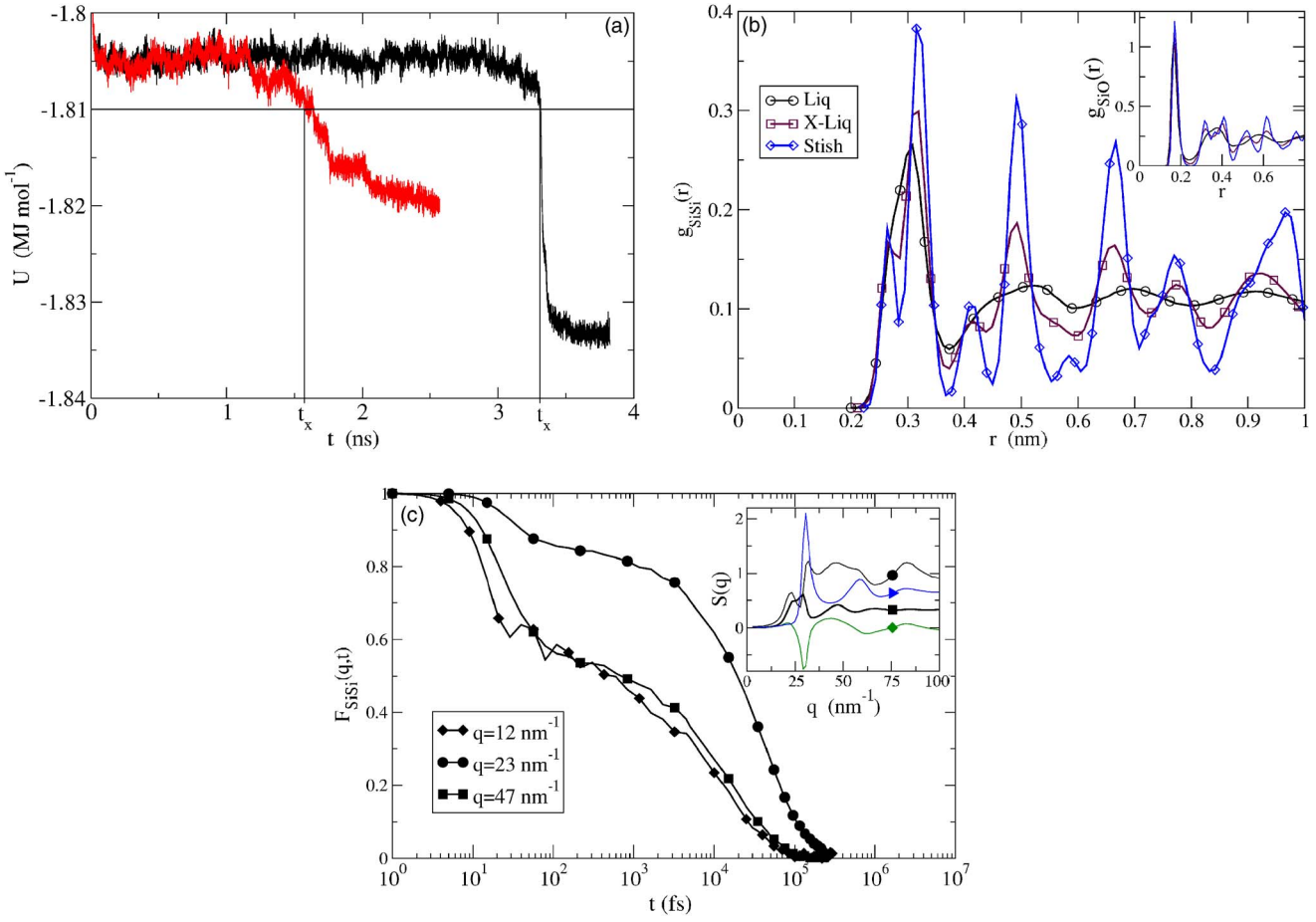

FIG. 3. (Color online) Crystalizing liquid. (a) Determination of t_x from the potential energy as a function of time. At $t=0$, the thermostat is reset from 5000 to 3000 K. When the system reaches a potential energy of $U_x=-1.81$ MJ/mol, it is well underway to crystallizing. (b) Structure at 3000 K as measured by $g_{\mathrm{SiSi}}(r)$ and $g_{\mathrm{SiO}}(r)$ (inset), of the liquid (Liq), the system after crystallization (X-Liq), and stishovite (Stish). (c) $F_{\mathrm{SiSi}}(q,t)$, the dynamic structure factor for Si atoms for three q. Inset shows the static structure factor $S(q)$ along with its components: total (circle), SiSi (square), OO (triangle), and SiO (diamond).

steady state liquid portions of the time series. With regards to the *NVE* simulations, we do not observe any significant differences in $F(q,t)$ or $S(q)$.

From $F_{\mathrm{SiSi}}(q,t)$, we see that the α-relaxation time for the system at V_0 and T_0 is approximately 100 ps. Thus, even though the system exhibits two-step (glassy) relaxation, the relaxation time is typically much shorter than the nucleation times and we are able to achieve a metastable liquid state.

If the fraction $R(t)$ of unnucleated systems obeys a simple first-order rate law, then the rate of nucleation J can be obtained from

$$\ln[R(t)] = -JV(t-t_0), \tag{7}$$

where V is the volume of the system and t_0 is the lag time, i.e., the time required to achieve a steady state of precritical nuclei.[25] However, to take advantage of Eq. (7) we must be able to identify the time when a particular system from our ensemble of runs has nucleated. Various methods can be used to detect crystallization such as examing the Voronoi volumes or counting the number of particle neighbors.[25] In this study, we contrast three approaches: first, we employ a simple energy criterion specific to the state point studied so that the crystallization time t_x for a MD run is the time at which the potential energy first reaches a value of $U_x = -1.81$ MJ/mol. That very few simulation runs reached U_x and then returned to a steady state liquid means that the system has progressed well past nucleation. In a sense, this mimics experimental measures which only identify a nucleation event by observing postcritical clusters that are growing. Second, we allow runs to continue 500 ps after the system reaches a lower potential energy of $U_{\mathrm{low}} = -1.82$ MJ/mol. Using U_{low}, we can also check the sensitivity of our rate calculation on the chosen energy threshold.

Our third criterion is based on identifying the critical nucleus. In Sec. IV, we find the size of the critical nucleus, using the cluster criteria outlined in the Appendix to identify an n-sized cluster, to be about 3. We can then define a new time, t_{nuc} as the latest time at which the largest cluster in the system $n_{\max} \leqslant 1$, i.e., the last time the liquid is precritical, and compare the nucleation rates based on our different criteria. By choosing $n_{\max} \leqslant 1$, we err on the side of making t_{nuc} a lower bound on the nucleation time.

Thus, we have three measures of the nucleation time: the time t_x it takes to reach a potential energy U_x indicative of the beginning of crystallization; the time it takes to reach a low energy threshold U_{low}; and the last time t_{nuc} at which the system possesses a largest cluster of size 1.

Figure 4 shows a plot of R using these three criteria R_x, $R_{\mathrm{low}}(t)$, and $R_{\mathrm{nuc}}(t)$, obtained using the upper and lower energy criteria and the critical cluster criteria, respectively, as a function of time. The slope of each of these functions is the same within the error suggesting that our rate calculation is not highly sensitive to the nucleation criteria, while the lag time, obtained from the intercept, is sensitive. Using t_x, we find that the 198 quenches from 5000 to 3000 K yield the shortest crystallization time of 0.28 ns, and the longest time of 10.53 ns, with an average time of 2.12 ns. The slope of the line of best fit is 0.60 ± 0.02 ns^{-1}, where we have omitted the data from times before 1 ns in the fit, and the time

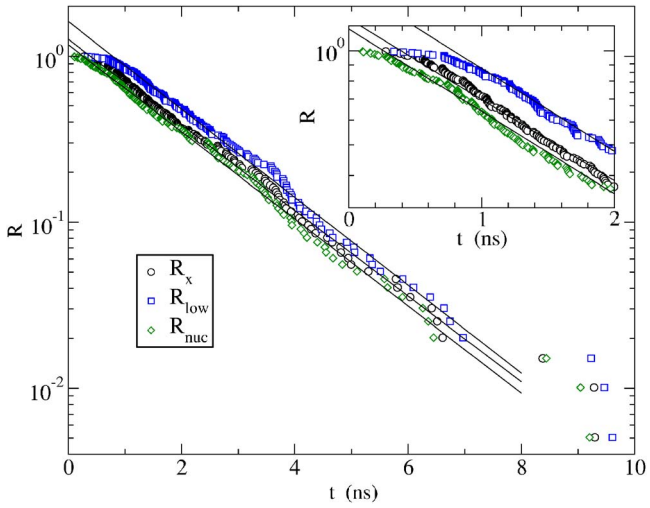

FIG. 4. (Color online) Determination of nulceation rate from R. The function R_x (circles) is shown here to be well described (except for very early times) by exponential decay with a rate constant of 0.60 ± 0.02 ns^{-1}, determined from the line of best fit. The data between 1 and 5 ns were used to obtain the fit. The functions $R_{\mathrm{low}}(t)$ and $R_{\mathrm{nuc}}(t)$ have the same slope to within uncertainty. Inset: Close-up at small t.

lag $t_0 = 0.4$ ns. Given that our cubic box length is 2.1627 nm, this yields a rate of $J = 0.059 \pm 0.002$ nm^{-3} ns^{-1} or 6×10^{34} m^{-3} s^{-1}.

We measure t_{nuc} in each of our 198 nucleation runs to a resolution of 0.005 ns and find a lower estimate of the lag time $t_0 \approx 0.260$ ns. The average time difference is $t_x - t_{\mathrm{nuc}} = 0.212$ ns, with a standard deviation of 0.117 ns. Comparing these two criteria, we find that the mean value of the largest cluster at t_x is $\langle n_{\max}(t_x) \rangle = 39$, i.e., about 10% of the system, with a standard deviation of 23. Therefore, for our system, the crystallization process significantly lowers the energy only when about 10% of the system has crystallized. We also note that in about 5% of the runs, the U_x criterion is triggered prematurely, i.e., a low-energy fluctuation goes below U_x, but then the system energy remains in steady state.

We note that calculating the rate directly from the slope of the plots in Fig. 4 may ignore the effects due to transient nucleation, i.e., that R decreases smoothly at early times instead of remaining at 1 until t_0,[25] so that our estimate of the rate and lag times are strictly lower bounds. Nevertheless, the independence of our slope on the nucleation criteria suggests that our calculation of the rate is robust and any corrections would be small.

Figure 5(a) shows a critical nucleus at 3300 K (obtained from constrained MC simulations described later), while Fig. 5(b) shows a postcritical crystallite of size 23 from a MD simulation at T_0. Figure 5(c) shows a representative configuration at the end of a crystallization simulation. These pictures provide a visual confirmation that the liquid does indeed crystallize to stishovite; that small nuclei (at least for $n_{\max} \geqslant 10$) resemble the bulk phase; and that the procedure used to define clusters is able to track the nucleation process.

IV. CNT CALCULATIONS

A. Free energy barrier

The central quantity of CNT is $N(n)$. However, it is not feasible to obtain $N(n)$ through direct simulation for two rea-

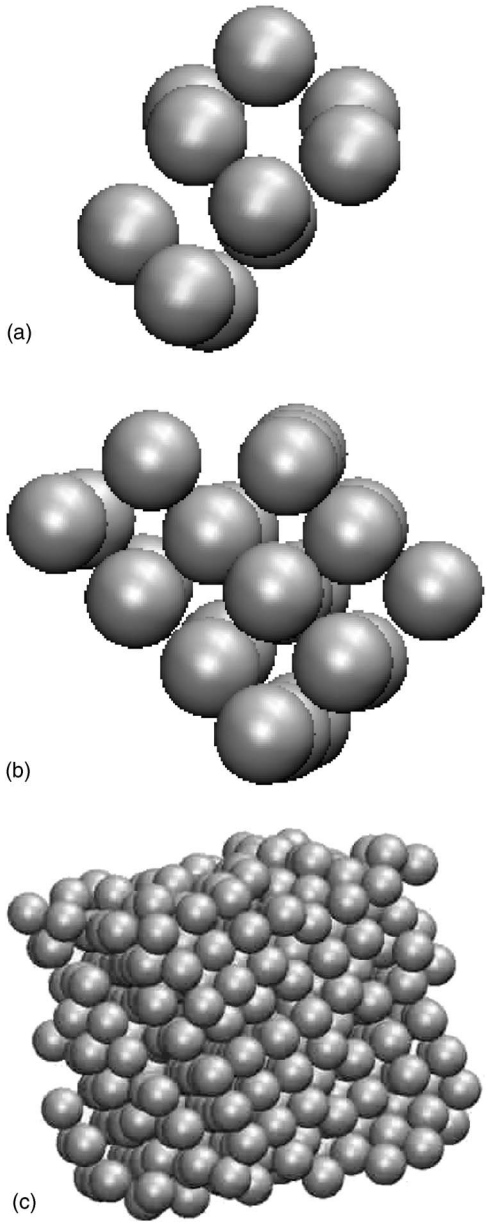

FIG. 5. Top: Sample critical nucleus at 3300 K containing ten Si atoms. Middle: A snapshot of the growing crystal embryo from a dynamic crystallization simulation at 3000 K when it contains 23 Si atoms. Bottom: Sample end configuration of a crystallization simulation.

sons: critical clusters are typically rare, and hence it is difficult to gain statistics; and after the formation of the critical cluster, the system irreversibly evolves toward the crystalline state. To overcome this, we add a bias to the system Hamiltonian which constrains the clusters of interest into existence. The new constrained Hamiltonian is then

$$H_C = H_{\mathrm{BKS}} + \phi(n_{\max}), \tag{8}$$

where H_{BKS} is the unbiased Hamiltonian derived from our BKS potential and

$$\phi(n_{\max}) = \frac{\kappa}{2}(n_{\max} - n_0)^2 \tag{9}$$

is the contraint with κ and n_0 being constants, and where $n_{\max}$, the size of the largest cluster in the system, is an order parameter.[10] The $N(n)$ measured under the constraint is then related to its value in the unconstrained system through the relation

$$\langle N(n)\rangle = \frac{\langle N(n)\exp[\phi(n_{\max})/k_BT]\rangle_C}{\langle \exp[\phi(n_{\max})/k_BT]\rangle_C}, \tag{10}$$

where $\langle\cdot\rangle_C$ denotes an average in the constrained ensemble. In the case where a cluster of size n is rare $N(n)=P(n_{\max})$, the probability that the largest cluster in the system is of size $n_{\max}$, Eq. (10) becomes

$$\langle P(n_{\max})\rangle = \frac{\langle P(n_{\max})\rangle_C \exp[\phi(n_{\max})/k_BT]}{\langle \exp[\phi(n_{\max})/k_BT]\rangle_C}. \tag{11}$$

It is important to note that our cluster definition ignores O atoms, and only uses Si atoms. Thus, a cluster of size n contains n Si atoms, or n SiO_2 units (see Appendix).

Since it is easier in practice to measure $P(n_{\max})$ than $N(n)$, we will use $P(n_{\max})$ interchangeably with $N(n)$ in the regime where the two are shown to be equal. Formally, this occurs when clusters are rare, and can be justified by the following. Let P_n be the probability that there is at least one cluster of size n in the system, and $P_n(i)$ be the probability that there are exactly i clusters of size n. Then,

$$P_n = P_n(1) + P_n(2) + P_n(3)\ldots, \tag{12}$$

$$N(n) = P_n(1) + 2P_n(2) + 3P_n(3)\ldots. \tag{13}$$

What we mean by a rare cluster of size r is that $P_r(1)$ is small, and additionally, that rare cluster appearance is independent of what other clusters are present, i.e., $P_r(2) \approx P_r(1)\times P_r(1)\approx 0$. This immediately leads to $P_n=N(n)$.[10,23] By extension, two rare clusters of different sizes appearing at the same time also occurs with vanishing probability $P_{r+m}(1)\times P_r(1)\approx 0$ [assuming $P_{r+m}(1)<P_r$ for $m>0$, i.e., larger clusters are rarer], and so a rare cluster will also be the largest cluster in the system. From these arguments, we obtain $P_n(1)=P_n=N(n)=P(n_{\max})$ for $n\geqslant r$ (the equality holds up to a normalization constant that is irrelevant in determining the free energy). Of course, when $N(n)\neq P(n_{\max})$, we measure $N(n)$ directly.

The basic MC scheme follows that presented in Ref. 26, where short *NVE* MD trajectories generate new configurations that are tested against the Boltzmann distribution. More explicitly, we begin with a configuration C_1 with the largest cluster $n_{\max}^{[1]}$. New random velocities drawn from the Maxwell distribution appropriate to the desired T are assigned to all the particles, and at this point the total energy is $H_{\mathrm{BKS}}^{[1]}$. With these new velocities, the system evolves along a constant *NVE* MD trajectory for ten time steps, with forces derived from H_{BKS}, to arrive at a new configuration C_2 with total energy $H_{\mathrm{BKS}}^{[2]}$ and largest cluster $n_{\max}^{[2]}$. With a perfect integration scheme, $H_{\mathrm{BKS}}^{[2]}=H_{\mathrm{BKS}}^{[1]}$. C_2 is accepted with propability p given by

TABLE I. Parallel tempering grids for three sets of simulations showing n_0 and T for each node, using a parabolic constraint on $n_{\max}$ with $\kappa=8$ kJ/mol (a) and $\kappa=16$ kJ/mol [(b) and (c)]. Each node is allowed to communicate with its nearest neighbor. For example, in (b), node 10 can attempt T-tempering switches with node 18, and n_0-tempering switch with nodes 9 and 11.

		n_0									
	T	1	3	5	7	9	11	14	17	20	25
(a)	3000	0	1	2	3	4					
	3100	5	6	7	8	9	10	11	12		
	3200	13	14	15	16	17	18	19	20	21	22
	3300	23		24		25		26	27	28	29
(b)	3100	0	1	2	3	4					
	3200	5	6	7	8	9	10	11	12		
	3300	13	14	15	16	17	18	19	20		
(c)	3000	0	1	2							
	3100	3	4	5							
	3200	6	7	8							

$$p = \min\left\{1, \exp\left[-\frac{1}{k_B T}(H_C^{[2]} - H_C^{[1]})\right]\right\}. \tag{14}$$

It is important to note that the acceptance criterion for this hybrid MD-MC method uses the total energy (kinetic plus potential), rather than just the potential.

With this hybrid MC method, it is only necessary to evaluate the cluster size distribution of the system at the end of each MD minitrajectory. The method also provides a way of incorporating the Ewald sums through multiparticle MD moves, i.e., energy changes arising from single particle moves are difficult to calculate efficiently when there are long range forces.

In order to facilitate equilibration, we employ parallel tempering over a matrix of runs having different values of n_0 and T. Our tempering scheme follows the descriptions given in Refs. 10 and 27. The particulars are as follows. Compute nodes running in parallel decide whether to attempt switches of configurations with neighboring nodes every ten MC steps, alternating between T-switch and n_0-switch attempts. For T switches, an attempt is made with each neighbor with a probability of 0.36. For n_0 switches, an attempt is made with each neighbor with a probability of 0.19. The probabilities for accepting switches are given in Refs. 10 and 27. In practice, it is computationally faster to switch Hamiltonians or T between processors, rather than configurations.

To gather data, we set up a grid of simulations with several values of n_0 for each T. Simulations are seeded from configurations sampled from the MD crystallization runs at T_0. To initially locate n^*, we set up a grid as given in Table I(a), with $\kappa=8$ kJ/mol. After equilibration, and after roughly determining the shape of the $\Delta G(n)$ curves, we set up other grids with $\kappa=16$ kJ/mol, as shown in Tables I(b) and I(c).

Our results for $T=3100$, 3200, and 3300 K come from Table I(b) and the run time is 700 000 MC steps. The starting configurations are those from Table I(a). $\Delta G(n)$ is calculated over the interval from 100 000 to 700 000 MC steps, checking that $\Delta G(n)$ as calculated separately from the intervals 100 000–400 000 and 400 000–700 000 MC steps do not show appreciable differences. For these T, $N(n) \approx P(n_{\max})$ for $n \geqslant 2$ and so we use $P(n_{\max})$ to determine $\Delta G(n)$. The first part of $\Delta G(n)$ is obtained by calculating $N(n)$ directly from simulations where n_0 is small. The simulation grid in Table I(c) provides a consistency check on the results for $T=3100$ K and $T=3200$ K. The run time is 350 000 MC steps.

Figure 6 shows pieces of $N(n)$ and $P(n_{\max})$ obtained from parallel simulations for $T=3200$ K and for various n_0. We see from the $n_0=1$ case that for $n \geqslant 2$, $P(n_{\max})=N(n)$. Therefore, only $P(n_{\max})$ need be calculated for determining $\Delta G(n)$ beyond $n=2$. Figure 6 also shows the consistency of the sampling between simulations of different n_0 near the top of the barrier. For each n_0, a portion of $N(n)$ is recovered up to a multiplicative constant, or additive constant in $\Delta G(n)$.

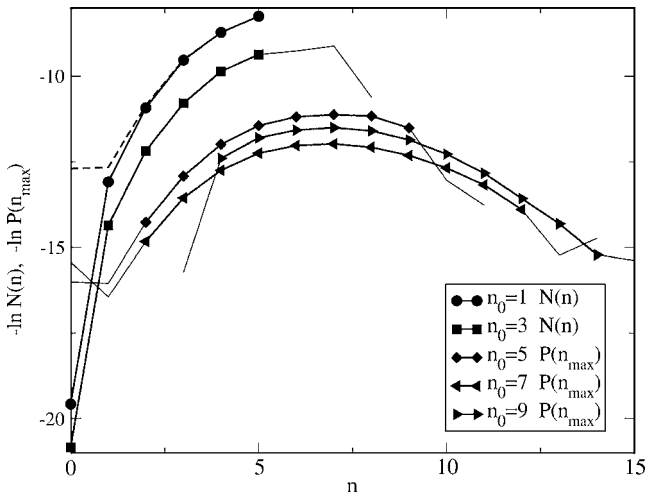

FIG. 6. Portions of $\Delta G(n)$ before shifting based on unnormalized histograms for $N(n)$ and $P(n_{\max})$. These are data transformed via Eqs. (10) and (11) from the constrained into the BKS silica ensemble. These distributions are for $T=3200$K, for processors 5–9 from Table I(b). The legend shows the values of n_0 used to constrain the system. The symbols and bold lines indicate portions of the data used to obtain the complete $\Delta G(n)$. For the cases of $n_0=1$ and 3, $N(n)$ is obtained directly. The dashed line shows $P(n_{\max})$ for the $n_0=1$ case, illustrating that already $N(n)=P(n_{\max})$ for $n \geqslant 2$. For larger values of n_0, $P(n_{\max})$ is used to obtain $\Delta G(n)$.

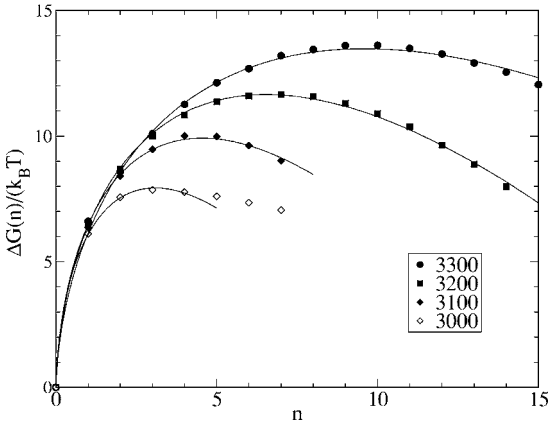

FIG. 7. $\Delta G(n)$ obtained from $N(n)$ after piecing together results from parallel simulations such as those shown in Fig. 6. The filled symbols are for the data described in Table I(b); open diamonds are for hard wall constraints described in Table II. The solid curves are fits to the form given by Eq. (2). For $T=3000$K only points with $n\leqslant 4$ are used for the fit. For $T=3300$ K, a one-parameter fit is shown: $\Delta\mu$ in Eq. (2) is obtained from independent calculations, and only a_{fit} is left to fit.

The pieces are matched using the self-consistent histogram method,[27] and the resulting $\Delta G(n)$ curve is shown in Fig. 7. The curves for $T=3300$ and 3100 K are produced by the same method.

B. Methodological challenges at $T=3000$ K

For $T=3000$ K, we encounter methodological difficulties using the parabolic constraint in our MC simulations, apparently due to the small size of the critical nucleus. At this T, as we shall see, $P(n_{\mathrm{max}})\neq N(n)$, and so we must find $N(n)$ directly, but the parabolic constraint together with Eq. (10) do not yield adequate statistics. For example, in Table I(c), node 0 infrequently samples states over the barrier, and because of the large factor of $\exp[\phi(n_{\mathrm{max}})/k_BT]$ in Eq. (10), these particular states dominate the resulting $N(n)$.

To obtain $N(n)$ at 3000 K, we replace the parabolic constraint with a vertical, hard wall potential by setting upper and lower bounds on n_{max}. Any MC move which violates $n^l_{\mathrm{max}}\leqslant n_{\mathrm{max}}\leqslant n^u_{\mathrm{max}}$ is rejected. Equation (10) is modified to simply be $\langle N(n)\rangle=\langle N(n)\rangle_C$ for $n^l_{\mathrm{max}}\leqslant n_{\mathrm{max}}\leqslant n^u_{\mathrm{max}}$, i.e., $N(n)$ is the same in the constrained and unconstrained ensembles within the upper and lower bounds on n_{max}. The constrained Hamiltonian in this case becomes

$$H_C = H_{\mathrm{BKS}} + \delta(n_{\mathrm{max}};n^l_{\mathrm{max}},n^u_{\mathrm{max}}), \tag{15}$$

where

$$\delta(n_{\mathrm{max}}) = 0 \quad \text{for } n^l_{\mathrm{max}}\leqslant n_{\mathrm{max}}\leqslant n^u_{\mathrm{max}} \tag{16}$$

$$=\infty \quad \text{otherwise}. \tag{17}$$

We then set up the hard wall simulation as outlined in Table II, taking initial configurations from Table I(c) and running for 1 400 000 MC steps. For each node, $N(n)$ is determined for $n^l_{\mathrm{max}}\leqslant n\leqslant n^u_{\mathrm{max}}$. Small windows in n are used to gather good statistics as well as to prevent nucleation in the bin closest to $n=0$. Error estimates are taken by considering different time intervals in determining $N(n)$. Ideally, $\Delta G(n)$ for $T=3100$ K should be the same when calculated either with hard wall or parabolic constraints. Any discrepancy between the curves is another measure of our uncertainty in $\Delta G(n)$.

TABLE II. Parallel tempering simulation grid showing T and limits on n_{max} for each node, using hard wall constraints. For a given node, only configurations with $n^l_{\mathrm{max}}\leqslant n_{\mathrm{max}}\leqslant n^u_{\mathrm{max}}$ are accepted during the MC simulation. Each node is allowed to communicate with its nearest neighbor. For example, node 1 can attempt T-tempering switches with node 7, and n_{max}-tempering switches with nodes 0 and 2.

	$n^l_{\mathrm{max}}-n^u_{\mathrm{max}}$					
T	0–2	1–3	2–4	3–5	4–6	5–7
3000	0	1	2	3	4	5
3100	6	7	8	9	10	11

As described above, we have calculated $\Delta G(n)$ for $T=3100$ K with three sets of simulations, as described in Tables I(b), I(c) and II. In Fig. 8 we plot as crosses the results from Table I(c), and see that the data show good consistency with those obtained from Table I(b), deviating only beyond $n=5$, the last n_0 in Table I(c). The hard wall curve also shows good consistency with the parabolic constraint results.

Figure 8 also shows that while $N(n)\approx P(n_{\mathrm{max}})$ holds for $T=3100$ K, it breaks down for $T=3000$ K, necessitating the direct calculation of $N(n)$ which we accomplish with our hard wall constraints.

However, despite the narrow binning of n_{max} outlined in Table II, all the bins at $T=3000$ K eventually nucleate. Figure 9 shows for node 0 in Table II the U and n_{max} time series [panels (a) and (b)] as well as early and late time distributions $N(n)$ [panel (c)] and $P(n_{\mathrm{max}})$ [panel (d)]. The U time series at first glance seems stable, but does show larger fluctuations at later stages than at the beginning. The n_{max} time series also shows a change in behavior: at early times (up to 400 000 MC steps) $n_{\mathrm{max}}=0$ or 1 is favored, while at later

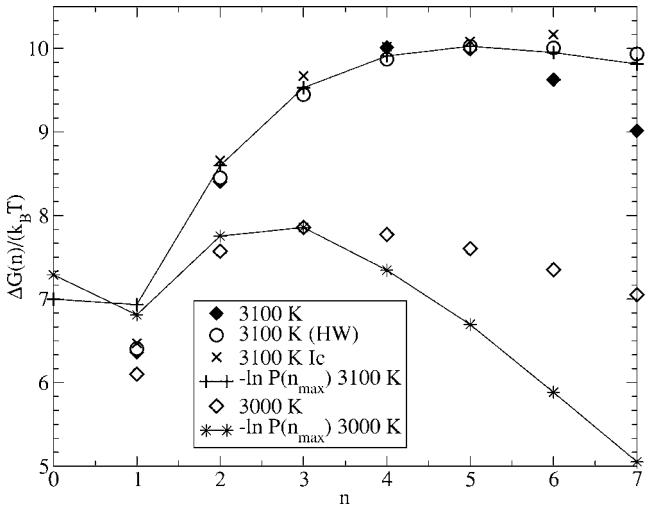

FIG. 8. (Color online) $\Delta G(n)$ obtained from $N(n)$ and $P(n_{\mathrm{max}})$ for $T=3000$ K, compared to results for $T=3100$ K. The open and filled diamonds represent the same data as in Fig. 7. The crosses show the results for $T=3100$K obtained from simulations in Table I(c), while open circles are from hard wall constraint simulations described in Table II. All three curves agree up to the critical size. The line connecting plus symbols (+) shows for Table II the approximate equality of $P(n_{\mathrm{max}})$ and $N(n)$ for $n\geqslant 2$. The line connecting stars (*) shows that this equality breaks down for $T=3000$ K.

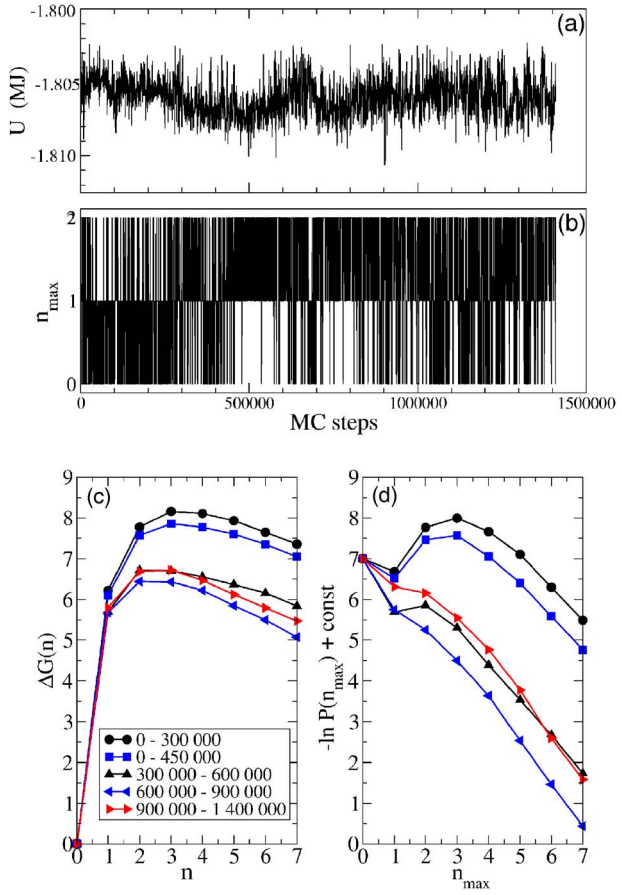

FIG. 9. (Color online) Breakdown of the n_{max} order parameter at $T=3000$ K. Time series are shown for node 0 in Table II for U (a) and n_{max} (b). In (a), U begins in a steady state similar to the unconstrained MD simulations at 3000 K (0-300 000 MC), and the following period of small decrease (300 000-500 000 MC steps) enters a regime with slightly larger fluctuations and where lower energy states are probed more often. Panel (b) shows a crossover near 400 000 MC steps to a regime where $n_{max}=2$ is favored over $n_{max}=0$. The effect on $\Delta G(n)=-\ln N(n)+\text{const}$ is shown in (c), where distributions taken from different portions of the time series are plotted: the early time profile is distinct from the later-time steady state. Panel (d) plots $-\ln P(n_{max})+\text{const}$, showing it to be monotonically decreasing at late times, apparently indicating a barrierless regime. However, it is more likely that the nucleation process is simply not adequately described by using n_{max} alone.

times $n_{max}=1$ or 2 is favored. The early and late time $N(n)$ profiles show a significant difference, as do the $P(n_{max})$ curves. In fact, at time beyond 500 000 MC steps, $-\ln P(n_{max})$ monotonically decreases.

Since n_{max} is an order parameter, the quantity $-k_BT \ln P(n_{max})$ is a free energy. The later-time curves shown in Fig. 9(d), therefore, would seem to indicate that there is no barrier to increasing n_{max} for the system, i.e., that the liquid is no longer a metastable phase. Alternatively, these data might suggest that it is no longer sufficient to describe the nucleation reaction coordinate solely in terms of n and that an additional parameter such as cluster quality may be needed.[28] For example, it could be the case that small clusters that are well ordered may be over the barrier, as indicated in the second half of the time series, while other less ordered clusters of the same size are on the liquid side of the barrier. Thus, for late times, this bin no longer contains the metastable liquid, but rather a postcritical state. The late-time

TABLE III. Fit parameters using Eq. (2) to describe the data as plotted in Fig. 7. The quantity $|\Delta\mu|/k_BT$ is not a fit parameter, and is determined in a way described in Ref. 21, within an error of ±0.08. The label 1-par indicates a one-parameter fit in which only a_{fit} is varied. Estimates of γ are obtained from a_{fit}, assuming a spherical nucleus.

T (K)	$\lvert\Delta\mu\rvert/k_BT$	$\lvert\Delta\mu_{fit}\rvert/k_BT$	a_{fit}/k_BT	γ/k_BT (nm^{-2})
3000	3.28	5.14	11.23	29
3100 (HW)	3.12	3.97	10.28	26
3100	3.12	4.36	10.84	24
3200	2.96	3.57	10.00	26
3300	2.81	2.87	9.08	23
3300(1-par)	2.81	2.81	8.96	23

$\Delta G(n)$ profiles, therefore, represent a lower bound of the CNT barrier for this T. The early time behavior, however, still shows a metastable liquid according to $-\ln P(n_{max})$ and is therefore used to estimate the CNT barrier. The curves for $T=3100$ K show no such difficulties.

These observations highlight the difficulty in determining $\Delta G(n)$ for such small values of n^*, where the quality of the cluster may significantly affect whether a cluster of a given size is postcritical. A possible solution is to introduce another order parameter that takes into account the quality of the cluster when determining free energy profiles.

Our main result from Fig. 8 is that we obtain $\Delta G(n)/k_BT=7.86\pm0.6$ for $T=3000$ K. The uncertainty is obtained by considering different portions of the (early) time series when constructing $\Delta G(n)$. We also obtain $n^*=3$ Si atoms (SiO_2 molecules) or ~9 atoms including O.

C. Comparison with CNT

Figure 7 shows the full $\Delta G(n)$ curves for the different T. We see from Fig. 7 that both n^* and $\Delta G(n^*)$ decrease as T decreases. Furthermore, we see that n^* ranges from 3 to 10. These small values make it unlikely that periodic boundary conditions induce catastrophic nucleation in our system.[29] Moreover, for $T=3000$ K we find $n^*=3$, and analyzing our MD simulation runs, we confirm that the energy (or pressure) signature of crystallization occurs after nucleation occurs, and that the creation of a critical nucleus at this T does not detectably affect the pressure.

The results in Fig. 7 allow us to compare the observed behavior to the form of $\Delta G(n)$ predicted by CNT, given in Eq. (2). We fit Eq. (2) to the data at each T, and determine the constants a_{fit} and $\Delta\mu_{fit}$ as fitting parameters. These fits are shown as solid lines in Fig. 7 and show that the functional form of Eq. (2) satisfactorily describes the data at all T. For $T=3000$ K, the fit is satisfactory only up to the top portion of the curve.

Next, given that the presence of the critical nucleus does not affect the system pressure, we calculate $\Delta\mu$ between stishovite and the liquid at the T and P of the liquid VT state point under consideration (calculated as the difference in Gibbs free energy per mole of Si, or SiO_2 unit), based on the results presented in Ref. 21. The values are presented in Table III, and compared to the corresponding values of $\Delta\mu_{fit}$. We find that $\Delta\mu_{fit}$ compares well to $\Delta\mu$ at $T=3300$ K, but

that differences appear at lower T, getting larger as T decreases. Thus, though the form of Eq. (2) fits the data for $\Delta G(n)$ at all T, the ability of CNT to predict $\Delta\mu$ is lost for $T<3300$ K.

Assuming that we have an approximately spherical nucleus, we estimate the surface tension from the fit parameter $a_{\rm fit}$ for our range of T to be $\gamma/k_BT\approx 25$ nm^{-2}; see Table III. Note that $a=4\pi(3/(4\pi\rho_n))^{2/3}\gamma$ for spheres. For silica at ambient P and near $T=1500$ K, experimental values for γ range from 0.3 to 0.7 J m^{-2}, or $\gamma/k_BT=15-34$ nm^{-2}.[30] For comparison, the value recently reported for NaCl at 800 K is $\gamma_{\rm NaCl}=80$ erg cm^{-2} or $\gamma_{\rm NaCl}/k_BT=7.2$ nm^{-2}. Thus, we see that at our high P and T, where the liquid is simpler, i.e., does not have a tetrahedral network, γ is still close in value to what it is at ambient P, and does not have a value closer to that of a simple ionic liquid. Table III also shows that despite the breakdown in the ability of CNT to predict $\Delta\mu$ in this T range, a fit of Eq. (2) to our $\Delta G(n)$ data still gives a relatively consistent estimate of γ.

Furthermore, it is interesting to note that while $\Delta\mu_{\rm fit}/k_BT$ changes some 80% as T decreases from 3300 to 3000 K, γ/k_BT roughly changes by only 25%. This perhaps indicates that the structure and/or density of the critical nucleus interior undergo larger changes with T than surface properties.

D. Kinetic prefactor

The crucial quantity in the kinetic prefactor is either λ or $f^+_{\rm crit}$ from Eqs. (4) and (5). Following the work of Frenkel and co-workers,[10,11] we calculate $f^+_{\rm crit}$ through Eq. (6). Equation (6) follows the assumption that the addition and detachment of particles from the near-critical crystallite are diffusive processes. In order to measure the deviation of the cluster size from the critical value, i.e., the right hand side of the equation, we isolate 80 clusters near the critical size from constrained MC simulations and use them to seed *NVE* simulations lasting 150 ps with randomized initial velocities corresponding to $T=3000$ K. We then use multiple time origins from each time series, where at each time origin the configuration has $n_{\rm max}=n^*$. In addition, to ensure that we are measuring the properties of clusters of critical size, each time origin is only chosen when the average cluster size for the preceding 1000 fs is between 2 and 4. Varying the averaging time or these upper and lower bounds does not appreciably affect the results.

We plot in Fig. 10(a) the quantity $\langle[n_{\rm max}(t)-n^*(0)]^2\rangle$. The plot shows a very rapid early time increase to a value of about 4 (inset shows early time behavior) or a fluctuation in size of the cluster of about two particles. Notwithstanding the early time change in $\langle[n_{\rm max}(t)-n^*(0)]^2\rangle$, we see that the time series enters into a diffusive regime that is linear in time, with $|n_{\rm max}(t)-n^*(0)|$ between 2 and 3. By fitting a line to this section, we obtain an estimate of the slope $m=(2.0\pm0.2)\times10^2$ ns^{-1}, which gives $f^+_{\rm crit}=m/2=(1.0\pm0.1)\times10^2$ ns^{-1}. This is about three times larger than the value obtained for molten NaCl at $T=825$ K and an atmospheric P of 0.033 ps^{-1}.[11]

The early time behavior of $\langle[n_{\rm max}(t)-n^*(0)]^2\rangle$ is plotted in the inset of Fig. 10(a) and shows a rapid increase corresponding to short-time fluctuations in the cluster size. These rapid fluctuations are seen in Fig. 10(b), where we plot a representative portion of an *NVE* simulation with a critical cluster in it. Although short-time fluctuations can be considerable given that $n^\star=3$, the general trend shown here suggests $n_{\rm max}$ fluctuates around $n^\star$.

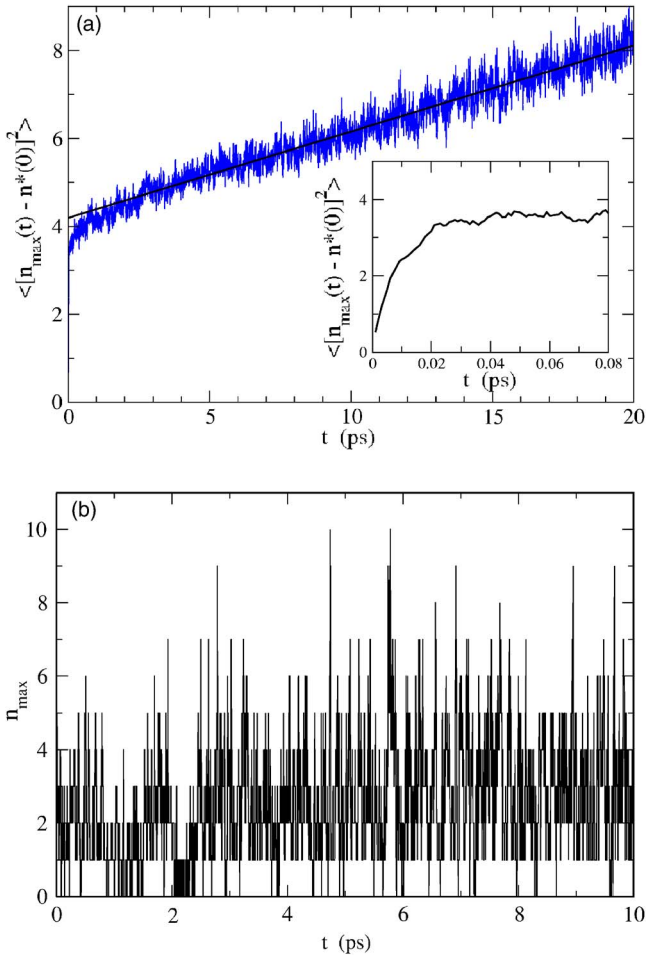

FIG. 10. (Color online) Calculation of $f^+_{\rm crit}$. Panel (a) shows a plot of $\langle[n(t)-n^*(0)]^2\rangle$ as a function of time at 3000 K. After a brief early time regime, the size of the cluster shows a diffusive behavior. The slope of the line of best fit in the linear regime is $(2.0\pm0.2)\times10^2$ ns$^{-1}=2f^+_{\rm crit}$. The inset shows early time behavior. Panel (b) shows $n_{\rm max}(t)$ for a portion of an *NVE* simulation seeded with a cluster of size $n^\star=3$.

All the factors required to calculate the nucleation rate via Eq. (3) are summarized in Table IV. The resulting rate is $J^{\rm CNT}=4.1\times10^{35}$ m^{-3}s^{-1}, and given the uncertainties in the calculated quantities, this result should be accurate within a factor of 2. Note that we have calculated the rate using $|\Delta\mu|$ as obtained from independent free energy calculations. It could be argued that $|\Delta\mu_{\rm fit}|$ is the appropriate quantity and this introduces an additional factor of uncertainty of $\sqrt{|\Delta\mu_{\rm fit}|/|\Delta\mu|}=1.25$.

The quantity λ can be obtained by solving Eqs. (4) and (5), resulting in

$$\lambda=\sqrt{\frac{24Dn^{*2/3}}{f^+_{\rm crit}}}. \tag{18}$$

Using our values for D, $f^+_{\rm crit}$ and n^*, we obtain $\lambda=0.20$ nm. To put this in perspective, the first peak of the Si–Si radial

TABLE IV. Summary of calculated quantities for $T=3000$ K.

Quantity	Value
n^*	3
$\Delta G(n^*)/k_BT$	7.86±0.6
f^+_{crit}	$(1.0\pm0.1)\times10^2$ ns^{-1}
$\lvert\Delta\mu\rvert/k_BT$	3.28±0.08
ρ_n	43.8929 nm^{-3}
D	$(8.0\pm0.2)\times10^{-8}$ nm^2 fs^{-1}
Z	0.241
λ	0.2 nm
J	6×10^{34} m^{-3} s^{-1}
J^{CNT}	4.1×10^{35} m^{-3} s^{-1}
J^{ms}	1.6×10^{34} m^{-3} s^{-1}

distribution function for the liquid at our state point is ≈0.3 nm and the width of the first neighbor peak in the liquid $g_{\text{SiSi}}(r)$ is about 0.1 nm.

E. Metastable equilibrium liquid $N(n)$

We now focus on the steady-state liquid that exists in our MD runs prior to any crystallization, which we call the metastable equilibrium liquid. We ask whether we can extract information about the barrier to nucleation from this metastable equilibrium liquid, i.e., without any constrained MC sampling.[31] To this end, we harvest configurations from our direct nucleation MD runs that have 500 ps$\leqslant t\leqslant t_x-500$ ps. This reasonably ensures that we have configurations only from the metastable liquid equilibrium, or steady state liquid, and have not included configurations that have begun to crystallize. We measure the distributions of cluster sizes to obtain $N^{ms}(n)$ and then define the free energy

$$\Delta G^{ms}(n) = -k_BT \ln N^{ms}(n) + \text{const}, \tag{19}$$

where the constant is chosen to ensure $\Delta G^{ms}(0)=0$. One might expect the two distributions $N(n)$ and $N^{ms}(n)$ to be the same. However, $N(n)$ is obtained by allowing otherwise unstable clusters to equilibrate in the surrounding liquid, while $N^{ms}(n)$ is obtained directly from a dynamic simulation. Furthermore, the way we obtain $N^{ms}(n)$ reduces sampling of states near the top of the barrier.

We plot $\Delta G^{ms}(n)$ in Fig. 11(a) (filled circles). Although the first part of the data behaves like a usual barrier, the curve at larger n is straight. A linear $\Delta G^{ms}(n)$ implies an exponential $N^{ms}(n)$. It also implies that the work required to add a particle to the cluster is independent of n. Clearly, this does not fit the CNT picture, where increasing the size of the cluster reduces the work required to add a particle.

In order to extract some information from $\Delta G^{ms}(n)$, we calculate the quantity $[\Delta G^{ms}(n)+\lvert\Delta\mu\rvert n]/k_BT$, which should be a linear function of $n^{2/3}$, and plot it in Fig. 11(b). The resulting curve does indeed show a linear dependence on $n^{2/3}$ at small n. A fit through the origin using the first four nonzero data points yields a slope of 9.2. Using this slope, we construct the CNT curve $C^{ms}(n)=-\lvert\Delta\mu\rvert n+9.2n^{2/3}$ and plot it in Fig. 11(a) (solid line). From this curve, we obtain $\Delta G^{ms}(n^*)=10.74$ and $n^*\approx6$. Using these parameters, while keeping f^+_{crit} as calculated earlier, we obtain an estimate of the nucleation rate of $J^{ms}=1.6\times10^{34}$ s^{-1} m^{-3}, a value closer to J than that obtained from $N(n)$ (see Table IV).

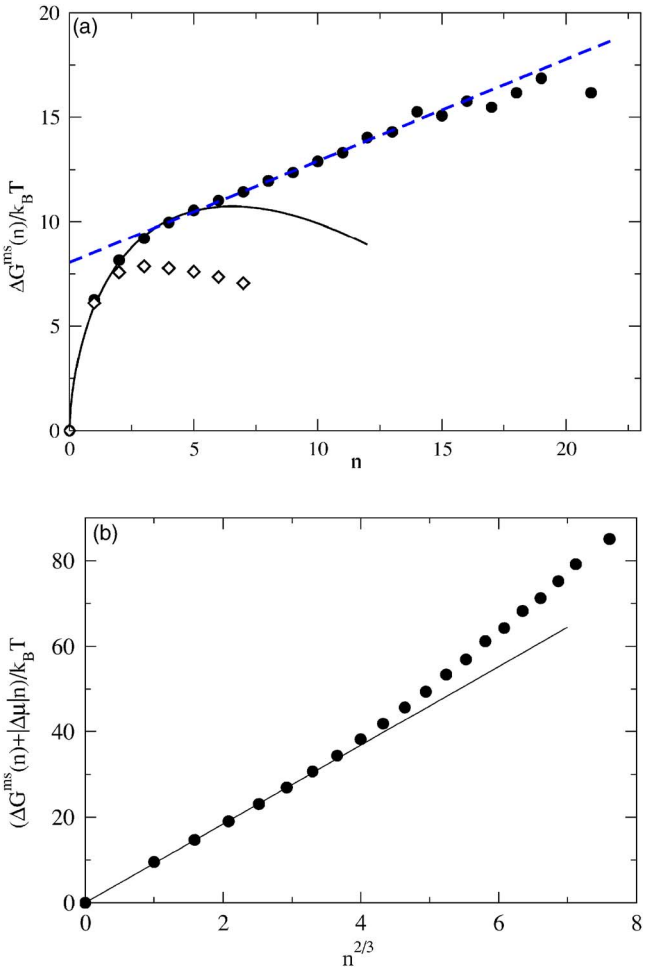

FIG. 11. (Color online) Work of cluster formation at $T=3000$ K derived from $N^{ms}(n)$ distributions obtained directly from NVT MD simulations where no crystal nucleation has occurred. Panel (a) shows $\Delta G^{ms}(n)/k_BT$ (filled cirles) along with the equilibrium $\Delta G(n)/k_BT$ (open diamonds), the curve $(-\lvert\Delta\mu\rvert n+9.2n^{2/3})/k_BT$ (solid curve), and a fit of the linear part of $\Delta G^{ms}(n)/k_BT$ at high n. Panel (b) shows the quantity $[\Delta G^{ms}(n)+\lvert\Delta\mu\rvert n]/k_BT$ that according to Eq. (2) should be a linear function of $n^{2/3}$. The line of best fit is constrained to pass through the origin, and has slope 9.2, as obtained by fitting to the first four nonzero data points.

This close agreement with J still leaves us with the question of why $\Delta G^{ms}(n)\neq\Delta G(n)$. In Fig. 11(a), we plot for comparison $\Delta G(n)$ and see that it is significantly lower than $\Delta G^{ms}(n)$.

V. DISCUSSION

In this study, we take advantage of a liquid state point that spontaneously nucleates on a time scale long enough to allow the determination of the properties of the metastable liquid. By sampling many nucleation events, we obtain the rate directly as shown in Fig. 4, where we show that the nucleation process enters a regime of first-order kinetics. The criterion used to determine when nucleation has taken place, whether an energy criteria or an examination of the cluster size, does not significantly alter our estimate of the rate.

With the direct rate in hand, we wish to test the prediction of CNT. First, we calculate $\Delta G(n)$ for a series of T

above and including T_0. As is defined in Eq. (1), $\Delta G(n)$ is only formally a (relative) free energy for the case when n-sized clusters are rare. In such a case, $\Delta G(n)$ becomes equivalent to $-\ln P(n_{\max})$, which is formally a free energy. However, $N(n)$ is the quantity of central importance in CNT, and the interpretation of $\Delta G(n)$ as a free energy, and $\Delta G(n^*)$ as a free energy barrier, is valid for more moderate supercooling or for liquid condensation from the supersaturated vapor.

In this work, we probe T low enough that a considerable (small n) portion of $N(n)$ is not equivalent to $P(n_{\max})$. Indeed, at $T=3000$ K, where the small value of n^* makes all cluster sizes of interest sufficiently common, $N(n)$ and $P(n_{\max})$ are different everywhere. This does not affect the formalism of CNT, merely the identification of $\Delta G(n)$, as defined in Eq. (1), as a free energy.

This becomes important at $T=3000$ K, where it is difficult to keep the metastable liquid from nucleating even at the smallest range of $n_{\max}$. At this T, the free energy barrier according to $P(n_{\max})$ is about $1.5k_BT$ [Fig. 9(d)]. The possibility of a spinodal-like loss of liquid stability to the crystal becomes a prominent possibility.[32] On the other hand, a set of criteria are used in order to distinguish liquid and crystal states. Thus, in a system where nucleation is taking place in a localized region, most of the system will still be labeled as liquid. Therefore, there will be more liquidlike particles (corresponding to $n=0$) than single crystal-like particles (corresponding to $n=1$), so that $\Delta G(n)$ will always show a barrier. Hence, if nucleation is unavoidable because of some spinodal processes, the usefulness of interpreting $\Delta G(n^*)$ as a free energy barrier is not clear.

With these thoughts in mind, we proceed to discuss the progression of $\Delta G(n)$ with T. At $T=3300$ K, the identification of $N(n)$ with $P(n_{\max})$ holds very well. The resulting $\Delta G(n)$ is well described by Eq. (2). Indeed, even the bulk value for $\Delta\mu$ calculated independently accurately describes the data, necessitating a fit only to determine the surface tension term. It is important to note that our approximation that the appearance of the critical nucleus does not affect P should be weakest at this highest T since the critical nucleus is largest. The $\Delta\mu$ result upholds our approximation.

The $\Delta G(n)$ profiles for $T=3200$ and 3100 K are similar to the 3300 K case, except that the bulk value of $\Delta\mu$ shows increasing deviation from $\Delta\mu_{\text{fit}}$. This deviation stems from either violating the assumption of cluster incompressibility used in the derivation of Eq. (2),[6,33] or from the (near certain) possibility that the structure of the small nuclei is different from bulk stishovite, and therefore follows a different equation of state (the bulk equation of state is used to calculate $\Delta\mu$).

Here, a note about ensembles is in order. Since we are at constant V, $\Delta G(n)$ [or $-\ln P(n_{\max})$ for that matter] represents a change in the Helmholtz free energy of the system. The use of $\Delta\mu$ in Eq. (2), however, is still formally correct.[34] Moreover, as we have shown, the critical nucleus does not significantly alter the P in our system. Hence, the nucleus can be regarded as being in either a constant V or a constant P environment.

At $T=3000$ K, clusters are insufficiently rare to identify $N(n)$ with $P(n_{\max})$. Therefore, we calculate $N(n)$ directly using hard wall constraints, a method giving the same results for 3100 K as those obtained from the parabolic constraint. Furthermore, we see a breakdown in the ability of our single order parameter $n_{\max}$ to sufficiently characterize the critical cluster. A high quality cluster of size 2 can be postcritical, resulting in what appears to be a spinodal-like profile in Fig. 9(d) for late times. For our current purposes, we use the portion of the time series which explicitly shows the metastable liquid state in order to calculate $\Delta G(n)$. In order to calculate $P(n_{\max})$ accurately at T near 3000 K, more stringent measures should be taken, including perhaps using an extra order parameter to help characterize the critical state better.

Calculating the kinetic components of the CNT expression for the rate, though more straightforward, requires comment. The parameter λ is usually defined as the distance a particle must diffuse when moving from the surrounding fluid to the nucleating phase, which is an intuitive interpretation in the case of condensation in a dilute gas. In the case of crystal nucleation, its meaning is not so clear, especially when we ask how λ should be interpreted with respect to a cluster criteria which identifies correlations between particle environments. Nevertheless, by calculating D and f^+_{crit}, we find $\lambda=0.2$ nm. This value is physically appealing, as it is less than the first neighbor Si–Si distance of 0.3 nm and the distance between the two subpeaks of the first $g_{\text{SiSi}}(r)$ peak for stishovite (the first peak is split) is about 0.1 nm. This reasonable value of λ is evidence that CNT provides an adequate description of nucleation in our system, a contrast to the case of molten NaCl, where λ was found to be unphysically large.[11]

Our calculation of f^+_{crit} suggests that are two time scales associated with the dynamics of the critical cluster. $[n_{\max}(t)-n^*(0)]^2$ grows rapidly over the first 40 fs before reaching a plateau near 4, after which, it increases at a much slower rate. The diffusive growth of the cluster occurs slowly and measurements of f^+_{crit} on the longer time scale lead to reasonable values of λ. The short-time fluctuations most likely arise from particles close to the cluster definition thresholds, for which small motions result in their being included or excluded in the crystalline cluster.

We emphasize that despite the difficulties at 3000 K, the rates J and J^{CNT} compare quite favorably, given similar comparisons done previously.[11] At higher T, there are no difficulties with the formalism used to calculate $\Delta G(n)$. Furthermore, the quantitative agreement between $\Delta G(n)$ and Eq. (2) is excellent, especially given the fact that $\Delta\mu$ is calculated independently for bulk phases.

Another intriguing aspect of this study is the difference between $\Delta G(n)$ and $\Delta G^{ms}(n)$. $\Delta G(n)$ is obtained through equilibrium simulations of the constrained system. The constraint allows for a rigorous determination on $N(n)$, allowing postcritical states to be sampled while determining the barrier. $\Delta G^{ms}(n)$ is determined through MD simulations of liquid quenched from $T=5000$ K to T_0, allowing the liquid to relax for several α-relaxation times, and collecting data only until 500 ps before crystallization is detected through the energy. Only three runs have $t_x - t_{\text{nuc}} > 500$ ps, with the largest

difference being 781 ps. Increasing the cutoff of the time series to 800 ps before t_x does not significantly alter $\Delta G^{ms}(n)$.

Thus, $\Delta G^{ms}(n)$ is constrained in a peculiar way. The data are pruned to include postcritical structures, so long as they happen to dissolve through some fluctuations. Therefore, postcritical states are sampled in a nonequilibrium fashion. Also, precritical fluctuations that happen to carry the system over the barrier quickly are not sampled well either. Therefore, near-critical states are sampled less often than in equilibrium [and hence $\Delta G^{ms}(n) > \Delta G(n)$]. We have not determined whether this sampling difference is sufficient to account for the difference between $\Delta G^{ms}(n)$ and $\Delta G(n)$.

Given these difficulties, the agreement between J and the rate calculated from $N^{ms}(n)$, following our seemingly logical procedure to obtain a barrier height from $\Delta G^{ms}(n)$ $[C^{ms}(n^*)]$, may be fortuitous. However, another possibility regarding the discrepancy between $\Delta G^{ms}(n)$ and $\Delta G(n)$ is that the time scale on which the $N(n)$ evolves is much longer than the α-relaxation time of the liquid. We note that quantities such as $g(r)$ and the structure factor are constant during the time 500 ps $< t < t_x - 500$ ps. However, it is possible that $N(n)$ evolves more slowly. In this case, the $N^{ms}(n)$ that we measure is not expected to be the same as $N(n)$, and is perhaps more physically relevant in calculating the rate. Perhaps this is why J^{ms} agrees better with J than does J^{CNT}. Clearly, the comparison of the metastable liquid distribution and the equilibrium distribution raises a number of interesting questions that warrant further investigation.

VI. CONCLUSIONS

We perform NVT MD simulations of liquid silica at $T_0 = 3000$ K and $V_0 = 4.5733$ cm^3/mol, corresponding to $P_0 = 44.0$ GPa, and calculate the rate of homogeneous nucleation to stishovite to be $J = (6.0 \pm 0.2) \times 10^{34}$ m^{-3} s^{-1}. This state point is located deep in the stishovite field in the PT phase diagram, and within the single phase coexistence region of stishovite in the VT phase diagram. T_0 is at about half the melting temperature at this P_0.

We also compare this rate to that predicted by CNT. The work in forming a cluster of size n $[\Delta G(n)]$ follows the form predicted by CNT [Eq. (2)] for $T = 3000$, 3100, 3200, and 3300 K. At 3300 K, an independent calculation of $\Delta\mu$ using bulk phase values allows for a successful one-parameter fit of $\Delta G(n)$. Assuming a spherical nucleus, an estimate for surface tension in this range of T is $\gamma / k_B T \approx 25$ nm^{-2}. At $T = 3000$ K, the CNT form only fits the data well only up to $n = 4$, one larger than the critical size. Furthermore, the usual identification $N(n) \approx P(n_{\max})$ breaks down strongly at this T.

We also find that $N(n)$ and $N^{ms}(n)$ differ. In fact, using N^{ms} yields a CNT result that is closer to direct measurement. This may indicate a subtle dependence of the nucleation rate on the initial T from which the system is quenched via slow evolution of the cluster distribution.

Calculating the kinetic prefactor, we obtain $f^+_{\mathrm{crit}} = 100 \pm 10$ ns^{-1}, resulting in a calculated rate of 4.1×10^{35} m^{-3} s^{-1}, with an uncertainty of a factor of 2. Therefore CNT overestimates the rate by an order of magnitude. The average distance that a Si atom must diffuse in attaching itself to a crystalline cluster is $\lambda = 0.2$ nm. This length is approximately twice the width of the first neighbor shell of the Si–Si radial distribution function. This value of λ is physically quite reasonable.

ACKNOWLEDGMENTS

We thank the StFX hpcLAB and G. Lukeman for computing resources and support, and acknowledge support from the AIF, the CFI, the CRC Program, and NSERC.

APPENDIX: DETERMINING CLUSTER SIZE

We only consider Si atoms in our sample when determining crystallinity. There are three reasons for this: Si and O atoms have different local geometry and so the analysis is made easier by looking only at the Si–Si structure; it is computationally faster to do so; and our order parameter does not track, and therefore does not influence, what the O atoms are doing, allowing for greater structural freedom during the constrained MC simulations.

In terms of determining local geometry, the difficulty arises in describing the different environments of Si and O atoms. In the case of NaCl, both species have the same coordination environment in the solid, and therefore can be described with one scheme. In the case of SiO_2, rather than finding a way of describing Si–O, O–O, and Si–Si bonds separately, we choose to account for Si atoms only. This is also computationally faster. We assume that the strong local stoichiometry will persist in the growing clusters as well.

In order to define a crystalline cluster forming within the liquid, we follow the procedure laid out in Ref. 7. We need a bond order parameter that captures crystal structure. To begin with, we use spherical harmonics $Y_{lm}(\hat{r}_{ij})$, where $\hat{r}_{ij}$ is a unit vector pointing along a bond between particles i and j (and thus providing elevation and azimuth angles with respect to a fixed coordinate system). For fcc and bcc crystals, $l = 6$ has been used, while for salt (having cubic structure), $l = 4$ has been used.[11] The first step is to define a local quantity on the particle level,

$$q_{lm}(i) = \sum_{j=1}^{N_b(i)} Y_{lm}(\hat{r}_{ij}), \tag{A1}$$

where the sum is over the N_b bonds of particle i. A global measure of the overall crystallinity can be written as

$$Q_{lm} = \frac{\sum_{i=1}^{N} q_{lm}(i)}{\sum_{i=1}^{N} N_b(i)}, \tag{A2}$$

and hence a quantity that does not depend on the coordinate system is

$$Q_l = \left(\frac{4\pi}{2l+1} \sum_{m=-l}^{l} |Q_{lm}|^2 \right)^{1/2}. \tag{A3}$$

Usually, N_b is determined via a cutoff distance near the

TABLE V. Q_l for $l=4$, 6, and 8, for various structures and choices of N_b: face-centered cubic (fcc), body-centered cubic (bcc), hexagonally close-packed (hcp), simple cubic (sc), liquid silica at $T=3000$ K (Liq), stishovite (ST) at 3000 K, stishovite at 0 K, and the structure that results when the liquid spontaneously crystallizes to stishovite at 3000 K (X-Liq).

Structure	N_b	Q_4	Q_6	Q_8
fcc	12	0.19	0.57	0.40
bcc	12	0.08	0.54	0.38
hcp	12	0.10	0.48	0.32
sc	6	0.76	0.35	0.72
sc	10	0.40	0.02	0.60
Liq	10	0.02	0.03	0.02
X-Liq	6	0.21	0.33	0.24
X-Liq	8	0.23	0.30	0.27
X-Liq	10	0.23	0.27	0.29
X-Liq	12	0.11	0.22	0.33
ST 3000 K	6	0.39	0.52	0.33
ST 3000 K	8	0.39	0.48	0.35
ST 3000 K	10	0.40	0.45	0.38
ST 3000 K	12	0.25	0.38	0.42
ST 0 K	10	0.41	0.51	0.42

first minimum in the radial distribution function. Ideally, fcc, bcc, and hcp structures have 12 neighbors, while simple cubic has six. However, during a simulation, N_b will fluctuate. In the present work, instead of defining a distance cutoff, we always choose the closest ten silicon neighbors of a given silicon atom, i.e., $N_b=10$ always. In stishovite, the first Si–Si neighbor shell contains ten atoms, although the shell is split with two neighbors slightly closer than the other eight.

In Table V, we list the Q_l values for $l=4$, 6, and 8, for various crystal structures as well as for both the metastable liquid and the state after the liquid has spontaneously crystallized (crystal with defects). We see that both Q_6 and Q_8 give high values for most crystals. However, $l=8$ seems to be less sensitive to the value of N_b chosen. In particular, for $N_b=10$ in the case of the simple cubic structure, Q_6 fares much worse that Q_8. For our study, we do not know what the structure of the precritical nuclei of stishovite is, and thus we prefer to have an order parameter that is more accepting of different structures. Therefore, we choose $l=8$

Having selected $N_b=10$, and $l=8$, we now proceed to determine what a crystal-like atom is, and whether two crystal-like atoms are part of the same cluster. Having defined q_{lm} in Eq. (A1), we can form a dot product c $(-1 \leqslant c \leqslant 1)$ between two neighboring Si atoms i and j as follow:

$$c_{ij} = \sum_{m=-8}^{8} \hat{q}_{8m}(i)\hat{q}^*_{8m}(j), \tag{A4}$$

where

$$\hat{q}_{8m}(i) = \frac{q_{8m}(i)}{(\Sigma_{m=-8}^{8}|q_{8m}(i)|^2)^{1/2}} \tag{A5}$$

and q^* is the complex conjugate of q. In this way, c is determined for every pair of neighboring atoms. For two atoms with very similarly oriented bonding geometry, c will have a value close to unity.

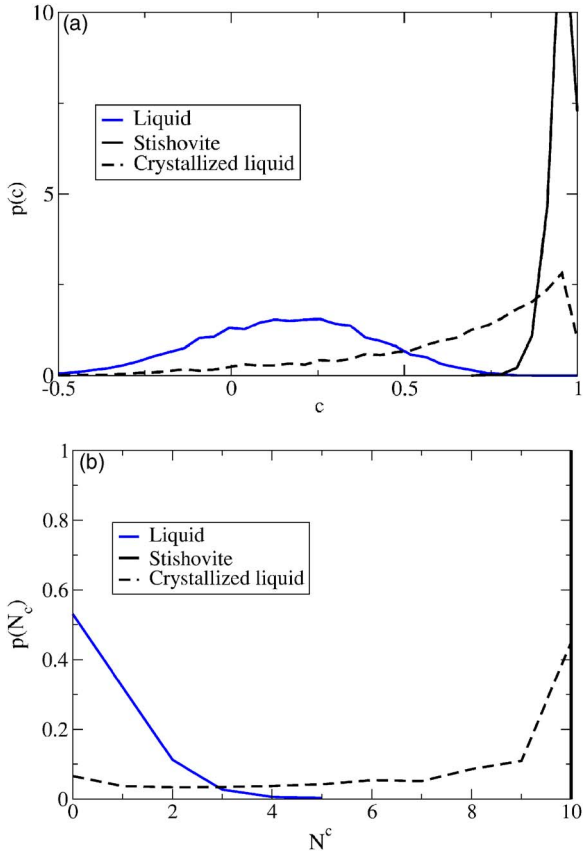

FIG. 12. (Color online) Determination of characterization thresholds. We plot the probability distribution of c_{ij} values in (a) for the liquid, stishovite, and the spontaneously crystallized liquid at T_0 and V_0. The results in each case are averages from five configurations. Based on this plot, we choose a value of $c_{\text{cut}}=0.5$. In (b) we plot the probability distribution of N^c values based on c_{cut}. At this T, stishovite appears to always have ten Si–Si connections per Si. Based on this plot, we choose a value of $N^c_{\text{cut}}=5$, at or above which a Si ion is deemed to be crystal-like.

The distribution of c values is plotted in Fig. 12(a) for stishovite, liquid, and spontaneously crystallized liquid all at T_0 and V_0. We see from the plot that very few atom pairs in the liquid have a value greater than about 0.75, while very few atom pairs in stishovite have a value less than 0.75. However, a value of $c=0.5$ provides a better criterion for differentiating between the liquid and the spontaneously crystallized configuration. Therefore, we choose a cutoff value of $c_{\text{cut}}=0.5$. A pair of neighboring atoms i and j that have $c_{ij} \geqslant c_{\text{cut}}$ are considered to be connected by a crystal-like bond.

To define a crystal-like atom, we say that the number of connections N^c an atom possesses must be greater than or equal to N^c_{cut}. To determine N^c_{cut}, we plot the distribution of N^c in Fig. 12(b) for the same cases as for c. We see that all atoms in the stishovite crystal have $N^c=10$, while the distribution for the liquid vanishes near $N^c=5$. From the plot, any value between 5 and 10 would serve to distinguish the liquid from the crystal. We choose $N^c_{\text{cut}}=5$ to be less restrictive in our choice of order parameter. Beyond this, clusters are defined by considering connections only between crystal-like atoms.

[1] J. W. Gibbs, *The Scientific Papers of J. Willard Gibbs* (Dover, New York, 1961).
[2] M. Volmer and A. Weber, Z. Phys. Chem. **119**, 227 (1926).
[3] L. Farkas, Z. Phys. Chem., Stoechiom. Verwandtschaftsl. **125**, 236 (1927).
[4] R. Becker and W. Döring, Ann. Phys. (Paris) **24**, 719 (1935).
[5] K. F. Kelton, *Crystal Nucleation in Liquids and Glasses* (Academic, Boston, 1991), Vol. 45, pp. 75–177.
[6] P. G. Debenedetti, *Metastable Liquids: Concepts and Principles* (Princeton University Press, Princeton, New Jersey, 1996).
[7] P. R. ten Wolde, M. J. Ruiz-Montero, and D. Frenkel, J. Chem. Phys. **104**, 9932 (1996).
[8] P. R. ten Wolde and D. Frenkel, J. Chem. Phys. **109**, 9901 (1998); P. R. ten Wolde, M. J. Ruiz-Montero, and D. Frenkel, *ibid.* **110**, 1591 (1999).
[9] S. Auer and D. Frenkel, Nature (London) **409**, 1020 (2001).
[10] S. Auer and D. Frenkel, J. Chem. Phys. **120**, 3015 (2004).
[11] C. Valeriani, E. Sanz, and D. Frenkel, J. Chem. Phys. **122**, 194501 (2005).
[12] M. Matsumoto, S. Saito, and Iwao. Ohmine, Nature (London) **416**, 409 (2002).
[13] M. Yamada, S. Mossa, H. E. Stanley, and F. Sciortino, Phys. Rev. Lett. **88**, 195701 (2002).
[14] H. Pang, Z. H. Jin, and K. Lu, Phys. Rev. B **67**, 094113 (2003).
[15] T. Motooka and S. Munetoh, Phys. Rev. B **69**, 073307 (2004).
[16] J.-M. Leyssale, J. Delhommelle, and C. Millot, J. Chem. Phys. **122**, 184518 (2005).
[17] K. K. Tanaka, K. Kawamura, H. Tanaka, and K. Nakazawa, J. Chem. Phys. **122**, 184514 (2005).
[18] B. van Beest, G. Kramer, and R. van Santen, Phys. Rev. Lett. **64**, 1995 (1990).
[19] J. Horbach and W. Kob, Phys. Rev. B **60**, 3169 (1999); I. Saika-Voivod, F. Sciortino, and P. H. Poole, Phys. Rev. E **63**, 011202 (2001); I. Saika-Voivod, P. H. Poole, and F. Sciortino, Nature (London) **412**, 514 (2001); A. Saksaengwijit, J. Reinisch, and A. Heuer, Phys. Rev. Lett. **93**, 235701 (2004).
[20] I. Saika-Voivod, F. Sciortino, and P. H. Poole, Phys. Rev. E **69**, 041503 (2004).
[21] I. Saika-Voivod, F. Sciortino, T. Grande, and P. H. Poole, Phys. Rev. E **70**, 061507 (2004).
[22] *Silica: Physical Behavior, Geochemistry and Materials Applications*, edited by P. J. Heaney, C. T. Prewitt, and G. V. Gibbs, special issue of Rev. Mineral. 62 (1994); N. R. Keskar and J. R. Chelikowsky, Phys. Rev. B **46**, 1 (1992).
[23] H. Reiss and R. K. Bowles, J. Chem. Phys. **111**, 7501 (1999).
[24] H. J. C. Berendsen, J. P. M. Postma, W. F. van Gunsteren, A. DiNola, and J. R. Haak, J. Chem. Phys. **81**, 3684 (1984).
[25] Y. Chushak, P. Santikary, and L. S. Bartell, J. Phys. Chem. A **103**, 5636 (1999); G. W. Turner, Y. G. Chushak, L. S. Bartell, *ibid.* **108**, 1666 (2004).
[26] B. Mehlig, D. W. Heermann, and B. M. Forrest, Phys. Rev. B **45**, 679 (1992).
[27] D. Frenkel and B. Smit, *Understanding Molecular Simulation: From Algorithms to Applications* (Academic, San Diego, 2002).
[28] D. Moroni, P. R. ten Wolde, and P. G. Bolhuis, Phys. Rev. Lett. **94**, 235703 (2005).
[29] J. D. Honeycutt and H. C. Anderson, Chem. Phys. Lett. **108**, 535 (1984).
[30] N. M. Parikh, J. Am. Ceram. Soc. **41**, 18 (1958); R. Brückner, J. Non-Cryst. Solids **5**, 123 (1970); N. P. Basal and R. H. Doremus, *Handbook of Glass Properties* (Academic, Orlando, 1986); P. J. Roberts, F. Couny, H. Sabert, *et al.*, Opt. Express **13**, 236 (2005).
[31] P. Beaucage and N. Mousseau, Phys. Rev. B **71**, 094192 (2005).
[32] L. F. Filobelo, O. Galkin, and P. G. Vekilov, J. Chem. Phys. **123**, 014904 (2005).
[33] P. G. Debenedetti and H. Reiss, J. Chem. Phys. **108**, 5498 (1998).
[34] D. Reguera, R. K. Bowles, Y. Djikaev, and H. Reiss, J. Chem. Phys. **118**, 340 (2003).